SYNTHESIS AND CHARACTERIZATION OF POLYMER NANOCOMPOSITES FOR ENERGY APPLICATIONS

A Thesis

by

WONCHANG PARK

Submitted to the Office of Graduate Studies of
Texas A&M University
in partial fulfillment of the requirements for the degree of

MASTER OF SCIENCE

August 2010

Major Subject: Mechanical Engineering

Synthesis and characterization of polymer nanocomposites for energy applications

SYNTHESIS AND CHARACTERIZATION OF POLYMER NANOCOMPOSITES FOR ENERGY APPLICATIONS

A Thesis

by

WONCHANG PARK

Submitted to the Office of Graduate Studies of
Texas A&M University
in partial fulfillment of the requirements for the degree of

MASTER DEGREE

Approved by:

Chair of Committee,	Choongho Yu
Committee Members,	Je-Chin Han
	Haiyan Wang
Head of Department,	Dennis O'Neal

August 2010

Major Subject: Mechanical Engineering

ABSTRACT

Synthesis and Characterization of Polymer Nanocomposites for Energy Applications.

(August 2010)

Wonchang Park, B. S., Korea Military Academy

Chair of Advisory Committee: Dr. Choongho Yu

Polymer nanocomposites are used in a variety of applications due to their good mechanical properties. Specifically, better performance of lithium ion batteries and thermal interface material can be obtained by using conductive materials and polymer composites. In the case of lithium ion batteries, electrochemical properties of batteries can be improved by adding conductive additives and conducting polymer into the cathode. Several samples, to which different conductive additives and conducting polymer were added, were prepared and their electrical resistance and discharge capacity measured. In the thermal interface material case, also, thermal properties can be enhanced by polymer nanocomposites. In order to confirm the thermal conductivity enhancement, samples were synthesized using different filler, polymer and methods, and their thermal conductivity measured. The influence of polymer nanocomposites and results are discussed and future plan are presented. In addition, reasons of thermal conductivity changing in each case are discussed.

DEDICATION

To my wife Nayoung Kim and daughter Christie

ACKNOWLEDGEMENTS

I want to thank my wife and my daughter for supporting and encouraging me. I am deeply indebted to my advisor Dr. Yu. Without his help, this thesis would not have been successful. I would like to thank Dr. Je-Chin Han and Dr. Haiyan Wang for consideration as committee members.

NOMENCLATURE

A	Area of cross section (m^2)
q	Heat transfer rate (W)
q_{avg}	Heat transfer average rate (W)
ΔT	Temperature difference (℃)
k	Thermal conductivity (W/m-K)

TABLE OF CONTENTS

CHAPTER Page

LIST OF FIGURES

Page

LIST OF TABLES

CHAPTER I

INTRODUCTION

Today, searching new energy sources is very important because amounts of fossil energy sources such as oil, coal and gas are limited. Solar energy source is a good candidate for new energy source because solar energy is unlimited and clean. However, solar energy needs energy conversion systems to use our real life. Figure 1 shows typical solar energy conversion system. In the solar energy conversion system, sunlight is collected by solar cells to use the solar energy. Then, solar energy is converted to electrical energy in the thermoelectric devices. During this procedure, heat originated from thermoelectric device moves to heat sink through TIM (Thermal Interface Material) in order to prevent overheating in the device. Electrical energy made from the thermoelectric device is stored in energy storage devices such as Li-ion batteries (lithium ion batteries). From the stored electrical energy in the battery, solar energy can be used in our real life. The performances of each part in the conversion system can be improved using a variety of methods. Among the conversion system, performance of TIM and Li-ion batteries can be enhanced using polymer-nanocomposites.

This thesis follows the style of Applied Physics Letters.

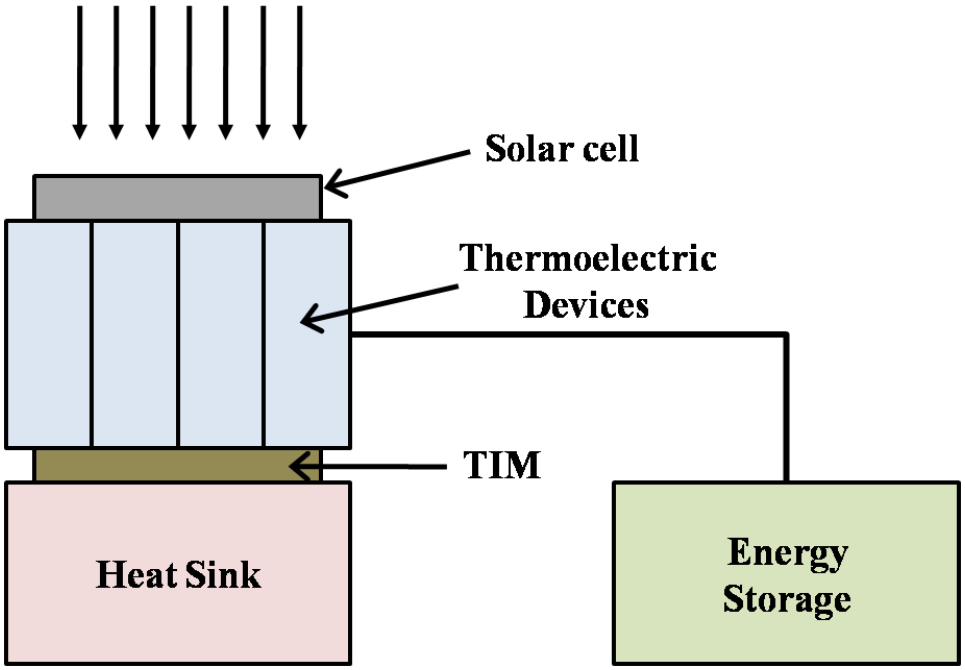

FIG.1. Schematic of energy conversion system

Many researchers are studying CNTs (carbon nanotubes) because of their outstanding mechanical properties [1], high thermal conductivity [2-4] and high electrical conductivity [5]. In addition, CNTs are very attractive materials due to their large aspect ratio [6]. However, CNTs are difficult to apply real life applications.

Polymers are used in a variety of applications because of their good mechanical properties and easy processing, but the thermal and electrical properties of polymers are not good enough for application in this field [7]. However, by making a polymer-nanocomposites, advantages of both CNTs and polymer can be obtained while reducing their disadvantages.

The TIM, performance can be improved using polymer-nanocomposites. The high thermal conductivity of CNTs and graphite and good mechanical properties of

polymer are key parameters for enhancing TIM performance. In addition, capacity and cycle ability of Li-ion batteries can be enhanced using CNTs-polymer composite. More conductive networks can be made by adding CNTs in a cathode active materials-polymer matrix. The performance of the cathode is improved by these conductive networks, so the capacity and cycle ability of the battery can be improved.

1.1 Lithium ion batteries

Lithium ion batteries consist of three main components; cathode, anode and electrolyte. During a charge and discharge process, reversible insertion and extraction of lithium ions occur in the cathode and anode materials through the electrolyte because of a reduction and oxidation (redox) reaction [8]. Equation (1) shows typical cathode half reaction and (2) shows anode half reaction in Li-ion batteries.

$$LiCoO_2 \leftrightarrow Li_{x-1}CoO_2 + xLi^+ + xe^- \quad (1)$$

$$xLi^+ + xe^- \leftrightarrow Li \quad (2)$$

Layered oxide materials such as $LiCoO_2$ and $LiNiO_2$ are the most commonly used materials in the cathode of Li-ion batteries [9]. $LiCoO_2$ has a rock salt lattice where the Li^+ and Co^{3+} ions order in the alternate (111) planes. Although $LiCoO_2$ have many advantages as a cathode material, there are a few disadvantages such as high cost and unstable structure when they are overcharged [10-12]. When $LiCoO_2$ is overcharged or experiences an excessive number of charge-discharge cycles, CoO_2 layers occur on the

electrode surface and cobalt of $LiCoO_2$ is dissolved in the electrolyte, decreasing the performance of the cathode $LiCoO_2$ is decreased [13-14].

$LiNiO_2$ has similar structure with $LiCoO_2$, but it is difficult to obtain a well ordered and stable structure [15-17]. In order to solve this problem, cobalt is added to $LiNiO_2$. By adding cobalt, $LiNi_{1-x}Co_xO_2$ has more stable structure and higher capacity than $LiNiO_2$ [18-19].

$LiMn_2O_4$ and $LiFePO_4$ are also good candidates for cathodes of Li ion batteries. The advantages of $LiMn_2O_4$ (spinel structure) are low cost, lack of toxicity and better thermal stability. However, $LiMn_2O_4$ has a lower discharge capacity than $LiCoO_2$ [18-19]. $LiFePO_4$ (phosphor-olivine structure) has a high theoretical capacity (170 mAh/g), voltage (3 ~ 4 V), but low cost and safety. However, the lithium extraction and insertion is limited to 0.6 Li^+/mol in $LiFePO_4$ [20]. Table 1 shows voltage and capacity of typical cathode materials.

Table. 1. Voltage and capacity of cathode materials [21]

Material	Voltage	Average capacity
$LiCoO_2$	3.7 ~ 4.1 V	140 mAh/g
$LiNiO_2$	3.5 V	180 mAh/g
$LiMn_2O_4$	4.0 V	100 mAh/g
$LiFePO_4$	3.3 V	150 mAh/g

A variety of materials can be used for the anodes of Li-ion batteries. Table 2 shows voltage and capacity of typical anode materials. Carbon and lithium are the best

candidate materials. Carbon is an attractive anode material because it is have light weight and has low electrochemical potential. In addition, carbon has a large theoretical capacity (372 mAh/g) [8]. However, there is an irreversible capacity during first charge-discharge cycle due to reaction with electrolyte. Furthermore, carbon anode can't be charged with some electrolytes such as propylene carbonate [8].

Lithium has very low electrochemical potential (0 V). However, because lithium is very reactive material, it makes oxidized surface on anode [8]. This oxidized surface can cause safety problems and cell failure.

Table. 2. Voltage and capacity of anode materials [22-23]

Material	Voltage	Average capacity
Li metal	0 V	•
Graphite (LiC_6)	0.1~0.2 V	372 mAh/g
Si ($Li_{4.4}Si$)	0.5~1 V	4212 mAh/g
Ge ($Li_{4.4}Ge$)	0.7~1.2 V	150 mAh/g

Lithium ions move between the cathode and anode in the electrolyte during the charge-discharge cycles. Liquid electrolytes consisted of organic solvents and lithium salts such as $LiPF_6$ and $LiClO_4$. A suitable electrolyte for Li ion batteries must have high ionic conductivity and high chemical stability. In addition, electrochemical stability to sustain the high voltage, low melting point and high boiling point are also important characteristics for suitable electrolyte [8].

Rechargeable lithium ion batteries are widely used in many applications such as cellular phones and laptop computers [24-25]. In addition, many devices such as electric vehicles need lithium ion batteries due to their high performances [26]. Therefore, Li-ion batteries should have the high capacity and good cycle stability in order to be used in these applications.

$LiCoO_2$ is the most popular among the possible cathode materials because it can be prepared easily [27]. However, this material has high conductive resistance due to high polarization. Thus, to improve the capacity and cycle performance of Li-ion batteries and create a conductive network in the cathode, conductive additives are needed [28]. In addition, by adding conducting polymer, performance of Li-ion batteries can be improved.

The commonly used conductive additives are carbon black and graphite powders [29-31]. Because these conductive additives have a high electrical property, they can make conductive bridges in the cathode, so performance of Li-ion batteries can be improved. In addition, some conductive additives like acetylene blacks can store large quantities of electrolyte in their structure [32]. However, networks of these conductive additives and active materials are easily broken because active material swell and shrink during charge and discharge [33]. Therefore, a search for new kinds of conductive additives that can retain conduction bridges without breaking during the cycle life is needed.

In order to improve conductive additives, many researchers have studied carbon nanotubes. CNTs can retain conduction bridges during charge and discharge cycles because CNTs have the good resilience and the electrical properties. Thus, capacity and

the life cycle of the Li-ion batteries can be improved by adding CNTs as conductive additives [34]. Many studies show that capacity retention ability of Li-ion batteries is enhanced when MWNTs (multi wall carbon nanotubes) are added into the cathode [33,35]. However, there are still a few studies using SWNTs (single wall carbon nanotubes) as the conductive additives. By using SWNTs as conductive additive, performance of Li-ion battery can be improved because of good electrical properties of SWNTs. In addition, performance of the cathode can be enhanced by mixing SWNTs and MWNTs.

Furthermore, performances of cathode can be improved using conducting polymer. Conducting polymers such as PEDOT:PSS (poly(3,4-ehylenedioxythiophene) poly(styrenesulfonate)) can be decorated on the surface of CNTs, so they can make more electrical network between CNTs [36]. Thus, more conduction networks in the cathode can be made using conducting polymer, so performance of Li-ion batteries can be improved using these networks.

The goal of this thesis is to improve performance of Li-ion batteries using several methods. In order to achieve this goal, capacity change of Li-ion battery will be studied changing conductive additives and adding a conducting polymer.

1.2 Thermal interface materials

Effective heat transfer by conduction is important to maintain and protect the performance of electronic devices. Good thermal contacts between devices such as heat sink and thermoelectric device can be accomplished by TIM. By filling the space

between two surfaces, TIM can offer better heat transfer. Figure 2 shows schematic of TIM between heat sink and thermoelectric device. Ideal TIM should have high thermal conductivity, minimal thickness and no leakage property. In addition, TIM should be non toxic and should maintain performance [37].

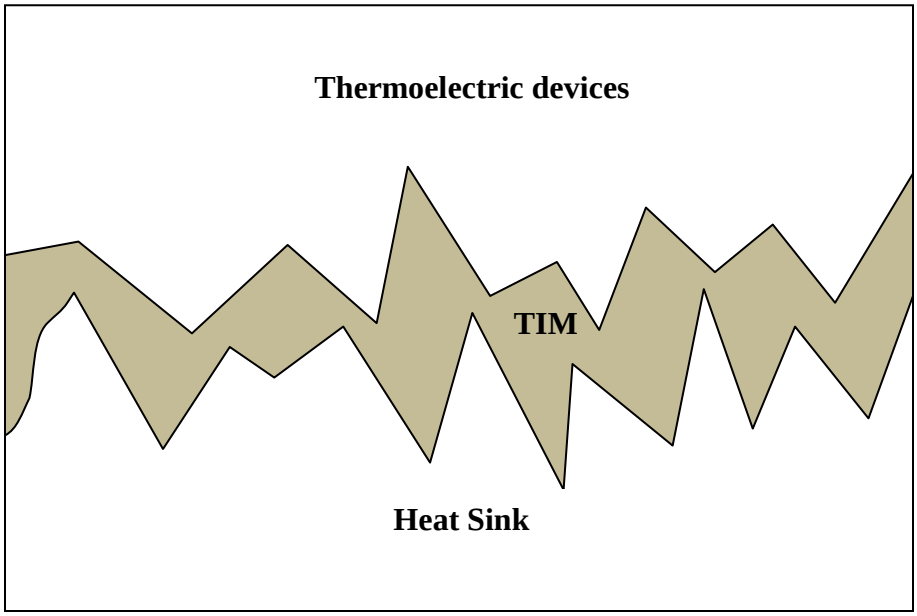

FIG. 2. Schematic of thermal interface material

Today, thermal grease, phase change materials and filled polymer are used as TIM in the many applications [37]. Thermal grease has several advantages such as high thermal conductivity and low cost. However, thermal grease is difficult to apply and remove and thickness control is difficult. In addition, it needs time to dry after being applied and may flow out when excess grease is used [37]. Phase change materials have high thermal performance and low thermal resistance. In addition, they do not need curing and dry out procedures and handling is easier than with thermal grease. However,

thermal conductivity of phase change materials is a little bit lower than grease. In addition, voids can be made during thermal cycles so it can bring discharge capacity decreasing [38-39]. Filled polymers are not messy and easy to apply. Also, they can sustain humid and other harsh environment. Nevertheless, thermal conductivity of polymers is lower than grease and they need curing procedures [37].

Today, to improve thermal properties and reduce the thermal resistance of TIM, a variety of attempts has been made. Specifically, many researchers have studied filled polymer as TIM because they have good mechanical properties although most polymers exhibit low thermal conductivity. Adding materials that have high thermal conductivity such as CNTs and graphite is a good approach for improving thermal conductivity of polymer.

Many studies have used CNTs to enhance thermal conductivity of polymer because CNTs exhibit a high thermal conductivity. The theoretical thermal conductivity of SWNTs has been demonstrated at ~ 6000 W/mK at room temperature [3]. In addition, thermal conductivity of isolated MWNTs was measured at ~ 3000 W/mK [4]. Thus, adding CNTs into the polymer is expected to enhance the high thermal conductivity.

Mixing with metallic particles which have high thermal conductivity and aligning CNTs in polymer are the most common methods to enhance thermal conductivity of CNTs-polymer composites [40-41]. However, high thermal conductivity has not yet been achieved [42-43]. Many researchers thought that strong interfacial phonon scattering between CNTs and polymer caused these results [42,44]. Nevertheless, CNTs are

still good candidate for TIM because of their high thermal conductivity, so many studies are continued with a variety of methods.

Adding graphite into polymer is also good candidate for better performance of TIM [45-46]. Thermal conductivity of polymer could be much enhanced by mixing with graphite [47]. These results were expected because flat surface of graphite can reduce the thermal interface resistance with polymer [48]. However, high contact pressure during application and low thickness are required for use graphite as TIM [45].

The goal of this work is to see a trend of thermal conductivity using different synthesis methods. In order to see a variety of trends, metal particle decorated CNTs-polymer composites were prepared to confirm the effects of using metal particles. In addition, graphite and CNTs were mixed in polymer to improve the performance and their optimal ratio was studied. Also, nanocomposites were prepared without surfactant to increase filler ratio in composites and different polymers were used to confirm the polymer effects.

CHAPTER II

EXPERIMENTAL PROCEDURES

2.1 Cathode of Li-ion batteries

2.1.1 Cathode synthesis

The cathode of a Li-ion battery consists of active material, conductive additive and polymer binder. $LiCoO_2$ (Alfa aesar, Co) was used as the cathode active material. MWNTs (multiwall carbon nanotubes, > 95 wt%) (Cheaptubes, Inc) and SWNTs (single wall carbon nanotubes, > 90 wt%) (Cheaptubes, Inc) are used as the conductive additives. SWNTs were soaked in NMP (N-mehtyl-2-pyrrolidinone) (Alfa aesar, Co) solution for 2 ~ 4 days in order to increase better dispersion in water. NMP soaked SWNTs were washed with heptanes (Alfa aesar, Co) and filtrated. Then, SWNTs were dried in the vacuum at 80 ℃ for 30 min to remove heptane.

PVdF (Polyvinylidone difluoride) (Kynar® HSV 900) and airflex @ 401 (Air Products, Inc) which is mixture of poly (vinyl acetate) and poly ethylene copolymer emulsion was used as the binder. NMP solution and DI water (de-ionized water) was used as solvent for cathode materials. PEDOT:PSS was added to improve conducting properties of the cathode. Airflex and DI water were used when PEDOT:PSS was used because PEDOT:PSS contained water. Because the boiling point of water is lower than that of NMP, water was boiled at low temperature in vacuum, so the cathode could not form a film shape. Thus, water based materials such as airflex, DI water and PEDOT:PSS were applied at lower temperature in order to prevent this problem.

$LiCoO_2$, conductive additives and polymer binder were mixed using a pen type sonicator in 2~3 ml of NMP solution. A 90 : 5 : 5 ($LiCoO_2$: conductive additives : binder) weight ratio was used in the no-PEDOT:PSS case. MWNTs only (5 wt%), SWNTs only (5 wt%) and MWNTs + SWNTs (2.5wt % + 2.5 wt%) samples were prepared to see the conductive additives effect for cathode. In with PEDOT:PSS case, 90 : 5 : 2.5 : 2.5 ($LiCoO_2$: conductive additives : PEDOT:PSS : binder) weight ratio was used. In this case, also MWNTs only (5 wt%), SWNTs only (5 wt%) and MWNTs + SWNTs (2.5wt % + 2.5 wt%) samples were prepared.

The mixed slurry was put on an aluminum foil and dried under the vacuum at 80 ℃. In the case of adding PEDOT:PSS, drying temperature was applied at 40 ℃ to prevent water boiling. Since the boiling point of water was decreased in the vacuum, a lower drying temperature was applied in order to avoid water boiling. After drying, top-bottom electrical resistance was measured with keithley 2000 multimeter to check enhancement of electrical properties. Figure 3 shows how the top-bottom electrical resistance of the cathode sample was measured.

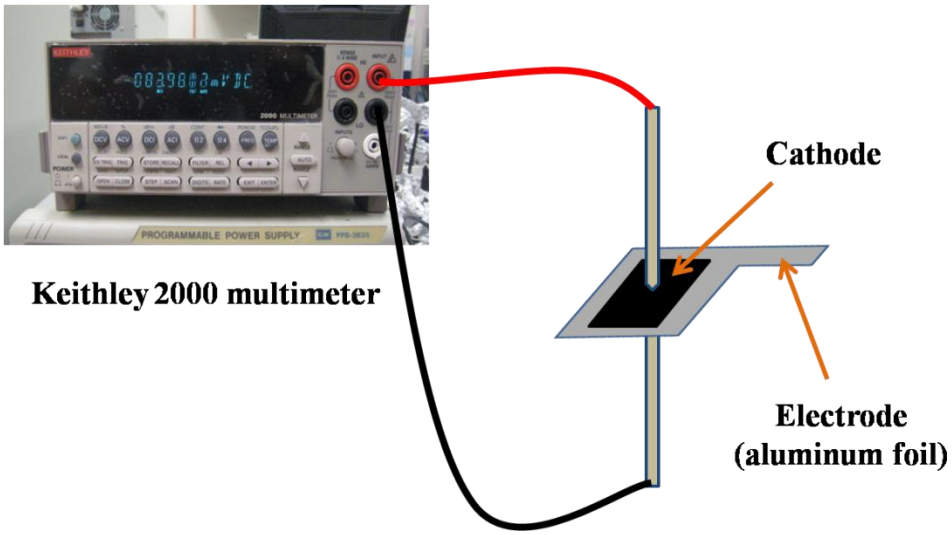

FIG. 3. Schematic of top-bottom electrical resistance measurement

2.1.2 Li-ion batteries assembly

The Li-ion cell was assembled to measure the electrochemical properties. A lithium metal foil (Alfa aesar, Co) as the anode, 1 M $LiPF_6$ (lithium hexafluorophosphate) (Alfa aesar, Co) in the volume ratio of 1:1 DMC (dimethyl carbonate) (Alfa aesar, Co) and EC (ethylene carbonate) (Alfa aesar, Co) as the electrolytes, 25 μm micro porous polypropylene film (Celgard® 2400) (Celgard, LLC) as the separator, acrylic plate as the case of the cell and the prepared cathode were used to assemble a cell. Cell assembly was conducted in the glove box. To remove air or water vapor, the glove box was filled with nitrogen gas and then gas in the glove box was purged with vacuum pump. Figure 4 shows Li-ion cell assembly procedures.

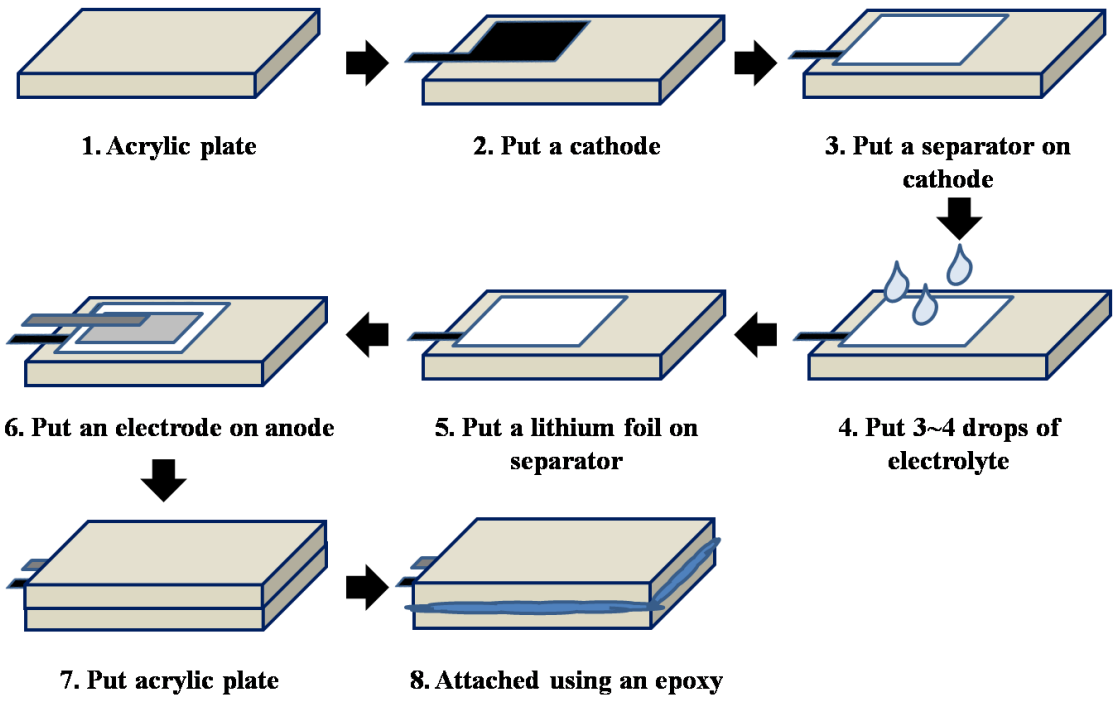

FIG. 4. Li-ion battery assembly procedures

2.1.3 Electrochemical properties measurement

The current change with time was measured with a keithley 2400 sourcemeter (Keithley, Co) and labview program controlled by computer during the charge and discharge. The capacity of the batteries was calculated as the time integral of the current flow from the beginning of time to the end time. Charge was conducted in constant current mode (0.2 mA) with 4.3 V compliance voltage for 1 hour. The sample was located in the safe box to prevent battery explosion during charge and discharge. Figure 5 shows measurement setup and on image of the safe box image. Electrical resistance of battery samples was measured by keithley 2000 multimeter to check adhesion between cathode and electrode and electrical properties.

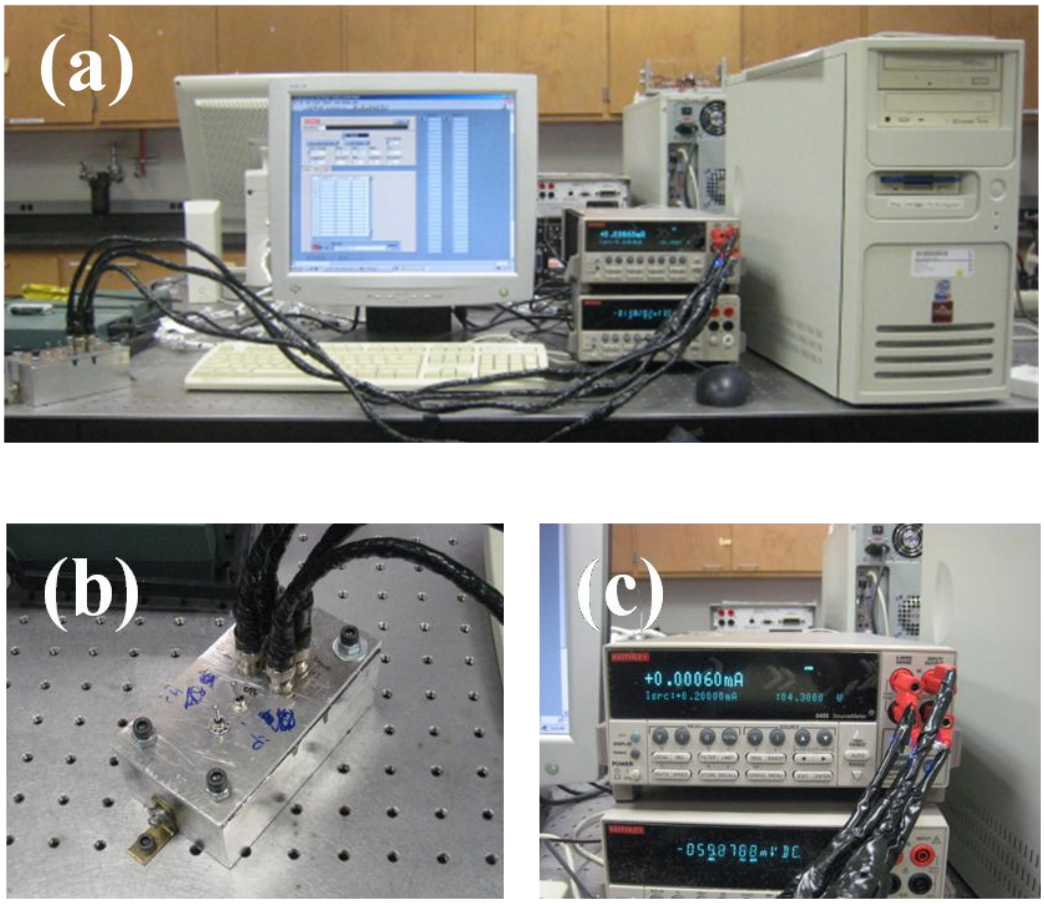

FIG. 5. Li- ion battery performance measurement setup (a) overall setup, (b) safe box for Li-ion battery, (c) Keithley 2400 sourcemeter

2.2 Thermal interface materials

2.2.1 Synthesis of metal particles decorated CNTs

DMF (Dimethylformamide) (Fisher, Co) solution was used to decorate iron particles onto the surface of MWNTs. First, MWNTs were refluxed in nitric acid (70 %) with stirring for 20 hours at 200 ℃. After refluxing, MWNTs were washed with DI water until pH changed to 7 and then filtrated with cellulose membrane to remove DI

water. Then, 0.15 g of washed acid treated MWNTs was dried in the fume hood for 2 days at room temperature. Acid treated MWNTs were put into 100 ml of DMF solution at 60 ℃ with stirring. After 30min, 100 ml of 0.02M iron nitrate (Acros organics, Co) solution was added into DMF solution and then mixed solution was kept for 16 h at 60 ℃ with stirring. Finally, mixed solution was filtrated and washed with DI water in order to remove DMF.

Hydrogen gas annealing process was used to decorate nickel particle onto surface of CNTs. 0.1 g of acid treated MWNTs was mixed with 100 ml of 0.05 M nickel nitrate (Fisher, Co) solution. Mixed solution was sonicated in a bath type sonicator and then stirred at room temperature for 20 hours with magnetic stirrer. The mixed solution was filtrated with cellulose membrane to remove DI water and then dried at 140 ℃ for 14 hours on a hot plate. After drying, the sample was treated at 500 ℃ for 3 hours in furnace in order to reduce H_2. Ramping and cooling was applied at 4 ℃/min with argon gas. TEM (transmission electron microscopy) (JEOL 1200 EX) was taken to observe the morphology of metal particle-decorated MWNTs.

2.2.2 Synthesis of CNTs and graphite-polymer nanocomposites

Different CNTs and graphite-polymer nanocomposites were prepared to confirm the thermal conductivity enhancement. The procedures of synthesis for CNTs and graphite-polymer nanocomposites for TIM are described below.

Filler such as CNTs and graphite and surfactants such as SDS (sodium lauryl sulfate) (Fisher, Co) or SDBS (dodecylbenzenesulfonic acid) (Acros organics, Co) were

mixed in the 65 ml HDPE plastic bottle (Fisher, Co). Surfactants were used to disperse CNTs in the DI water because CNTs are hydrophobic.

Next, 20 ml of DI water was added and then the mixed slurry was sonicated with a pen-type sonicator to disperse until perfectly dispersed. Subsequently, polymer binder such as airflex was added. Then slurry was sonicated for 2 ~ 3 minutes to mix with polymer binder. Mixed slurry was poured in a plastic container (5.4 cm × 5.4 cm × 1.7 cm) and then dried in the fume hood at room temperature for 2 ~ 3 days. Finally, the CNTs polymer composite was dried in the oven at 80 ℃ for 1 hour to remove DI water. Figure 6 shows overall procedures of polymer composites synthesis.

15 and 30 wt% MWNTs and 15, 30 and 50 wt% graphite samples were prepared to compare the MWNTs and graphite in thermal conductivity enhancement. In addition, MWNTs and graphite mixed samples (weight ratio: 4 : 1, 1 : 1, 1 : 4) were made to determine an optimal mixing ratio for the mixed filler case. Furthermore, samples using EPON 862 as polymer binder were prepared to compare samples using airflex.

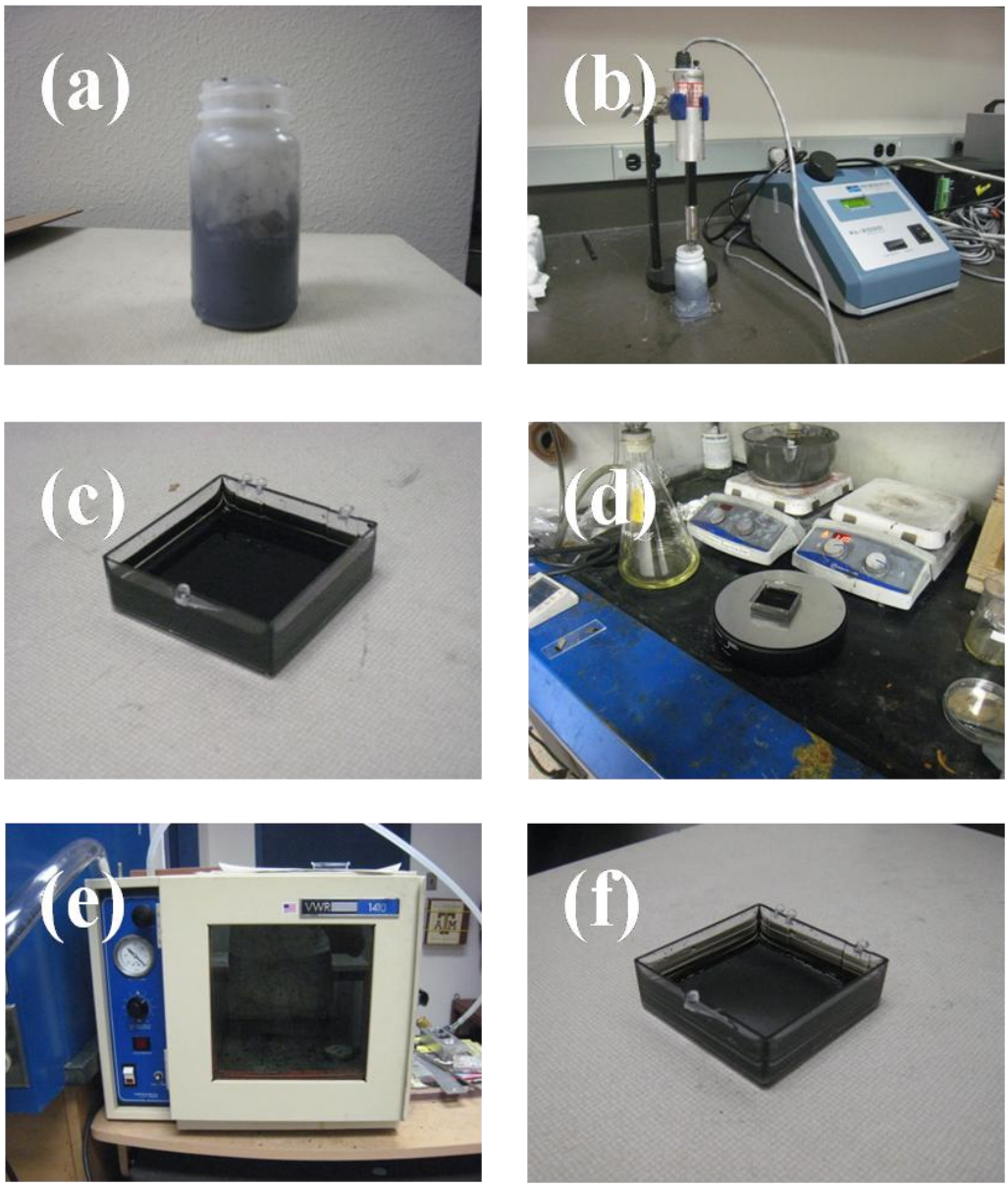

FIG. 6. Poymer nanocomposites making procedures (a) mix in the HDPE bottle, (b) sonication with pen type sonicator, (c) pour the solution into the plastic box, (d) drying in the fumehood, (e) drying at 80 ℃ in the oven, (f) sample after drying

Solvent such as DMF or NMP was used to make polymer composites without surfactant. The surface energies of DMF and NMP are similar to graphite [49-50]. As a

result, effective dispersion of filler is possible in these solvents because minimal energy is needed to break the van der Waals forces between nanotubes.

In order to synthesize the composite, first, CNTs and graphite were weighed and put into glass vial. Solvent was poured into vial and then sonicated with pen type sonicator until fillers were dispersed in the solvent. After dispersion, polymer binder was added and then sonicated for an additional 10 minutes. Figure 7 shows procedures of polymer composites synthesis without surfactant. In order to compare with the use of surfactant samples, 60 and 80 % graphite and 30 % / 30 % and 40 % / 40 % (wt ratio) of mixed MWNTs and graphite samples were prepared. Mixed slurry was poured into a cap of HDPE (high-density polyethylene) plastic bottle for drying. The cap was used as a drying container because the solvent attacked the plastic container which was used with the surfactant cases. In addition, a hydrophobic Teflon tape was attached on the cap to detach nanocomposites easily after drying. Samples were dried at 50 ℃ for 4 hours in the vacuum because solvent mist is toxic.

SEM (scanning electron microscopy) (JEOL JSM-7500 F) was taken of a cross-section of the sample to see the structure. Three sets of 10 thickness measurements each were taken and the average of each set was calculated. These averages were used to calculate the thermal conductivity. Differences in the thickness measurements were used for error calculation of thermal conductivity.

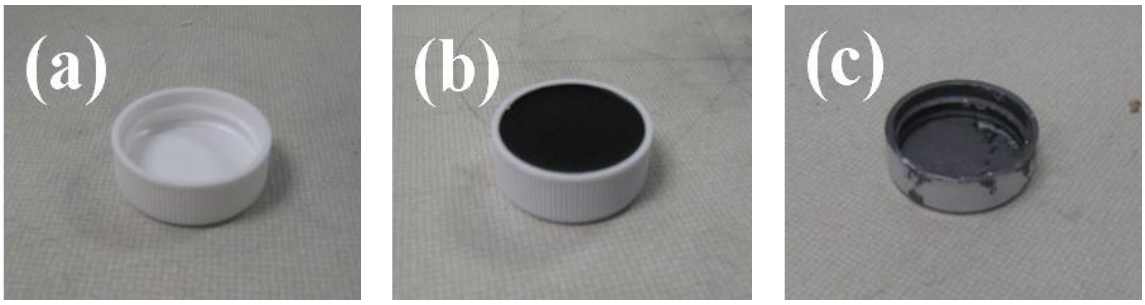

FIG. 7. Film preparation using solvents (a) cap with teflon tape, (b) pour mixed filler, polymer and solvents into cap, (c) sample after drying

2.2.3 Thermal conductivity measurement

Thermal conductivity can be measured using a steady state method. Figure 8 (a) shows the overall test setup and figure 8 (b) shows detail of the stainless steel rods and other test setup. As can be seen figures 8 and 9, the sample with 25.4 mm in diameter was located between two stainless steel rods. The upper brass part was maintained at 50 ℃ and the lower part at 0 ℃ for creating temperature gradients. A polymeric thermal insulator cover was used to reduce radiation and convection effect during measurement. Average temperatures at 1 ~ 10 points were measured using thermocouples after temperature was stable. Using the obtained temperatures and the distances between the points, upper and lower temperature of the joint section can be calculated.

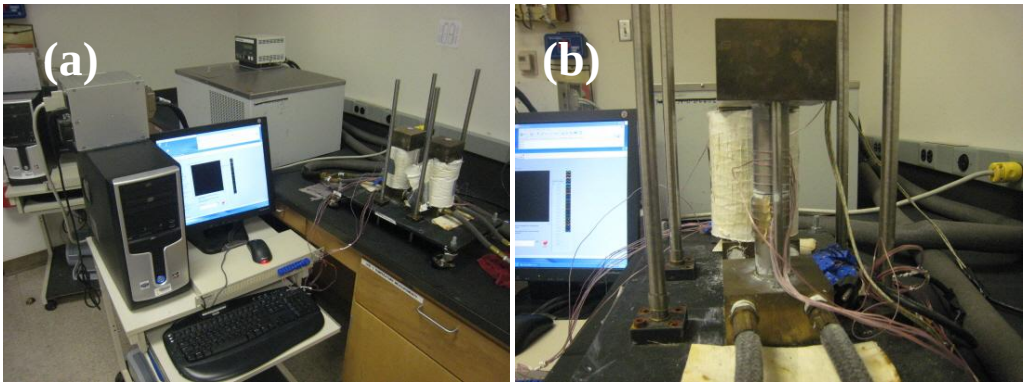

FIG. 8. Thermal conductivity measurement setup (a) overall measurement setup; computer, coolant system and measurement set (b) measurement set; stainless steel rod and brass part

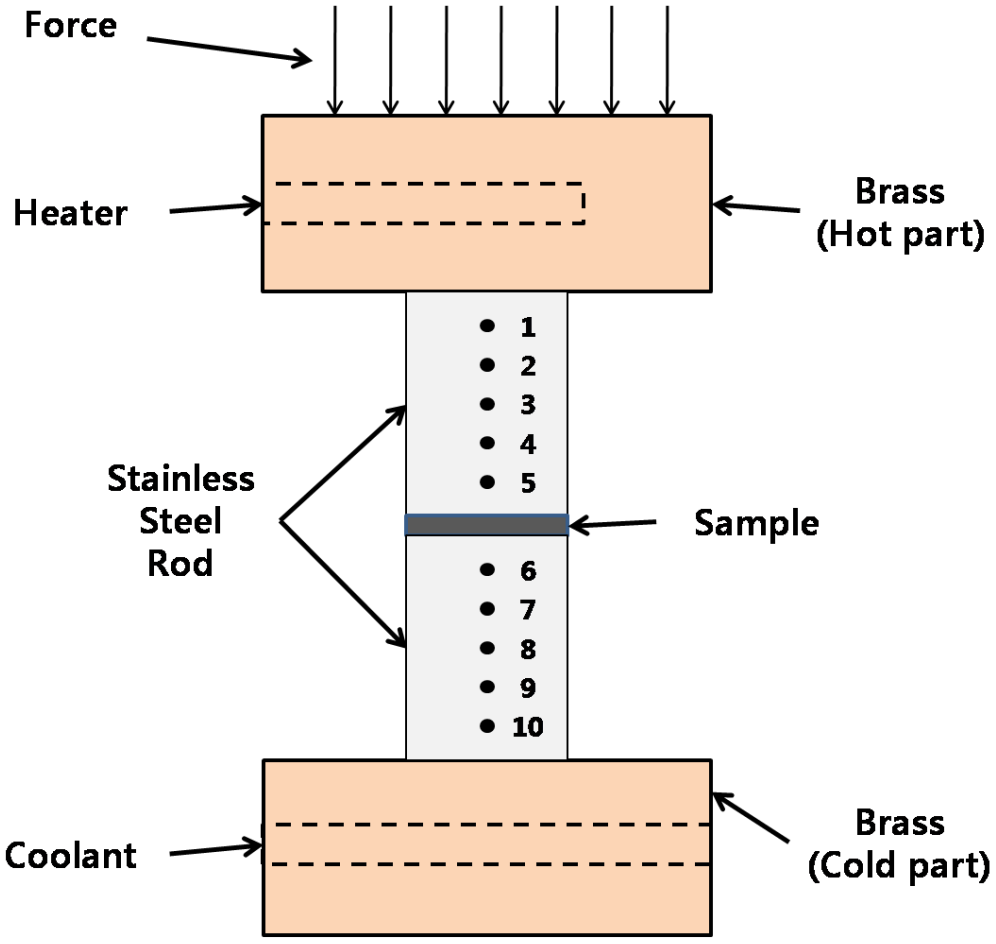

FIG. 9. Schematic of thermal conductivity measurement set-up

The temperatures of the upper and lower parts were measured without the sample in order to get the thermal conductivity of sample. After that, the thermal conductivity of the sample was measured. Figure 10 shows how one can calculate the upper and lower temperatures of joint section. After calculation of upper and lower part temperature, q (heat transfer rate, unit: W) and q_{avg} (average of heat transfer rate, unit: W) can be calculated using equation (3) ~ (5):

$$q_1 = k_{ss\ rod} \times A_{ss\ rod} \times \left(\frac{\Delta T}{\Delta x}\right)_{upper} \quad (3)$$

$$q_2 = k_{ss\ rod} \times A_{ss\ rod} \times \left(\frac{\Delta T}{\Delta x}\right)_{lower} \quad (4)$$

$$q_{avg} = (q_1 + q_2)/\,2 \quad (5)$$

$k_{ss\ rod}$ is the thermal conductivity of the stainless (unit: W/m•K) steel rod and $A_{ss\ rod}$ is the area of stainless steel rod (unit: m^2). $\left(\frac{\Delta T}{\Delta x}\right)_{upper}$ and $\left(\frac{\Delta T}{\Delta x}\right)_{lower}$ are the temperature gradients of the upper and lower stainless steel rods. ΔT (temperature difference, unit: ℃) can be obtained using equation (6):

$$\Delta T = T_1 - T_2 \quad (6)$$

Finally, thermal conductivity (k, unit: W/m•K) of sample can be obtained using equation (7):

$$k = \frac{(q_{avg} \times thickness\ \ of\ \ sample\ )}{\{A_{ss\ rod} \times (\Delta T_{sample} - \Delta T_{paste}\ )\}} \quad (7)$$

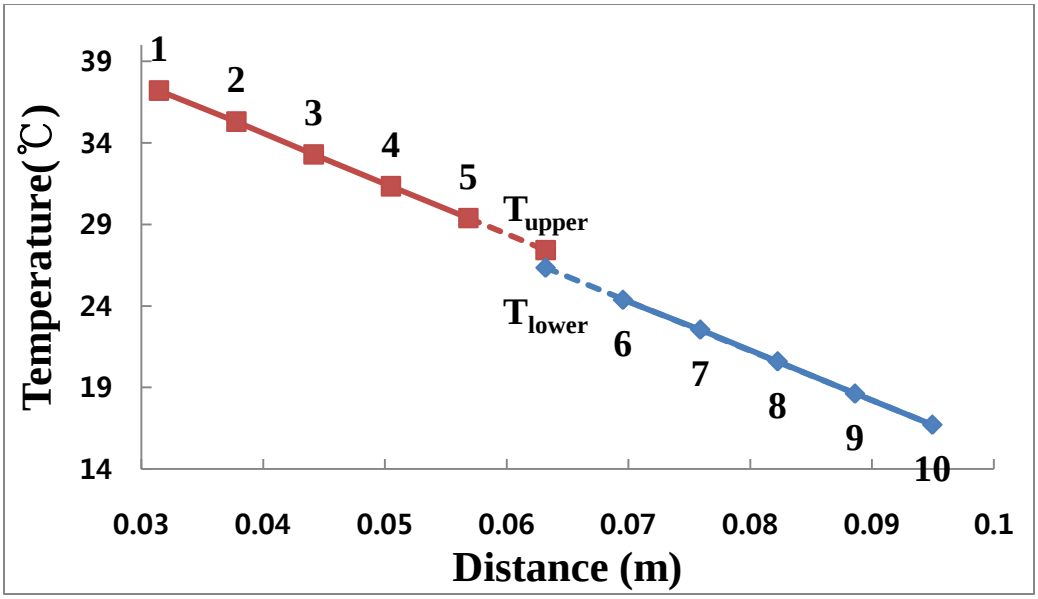

FIG. 10. Calculation upper and lower part temertaure of joint section using temperature gradient of stainless steel rods

CHAPTER III

RESULTS AND DISCUSSION

3.1 Cathode of Li-ion batteries

3.1.1 Top-bottom electrical resistance measurement

Electrical conductive network formation in the cathode is important for enhancing electrochemical performance. Top to bottom resistance of cathode samples was measured to check the electrical property enhancement.

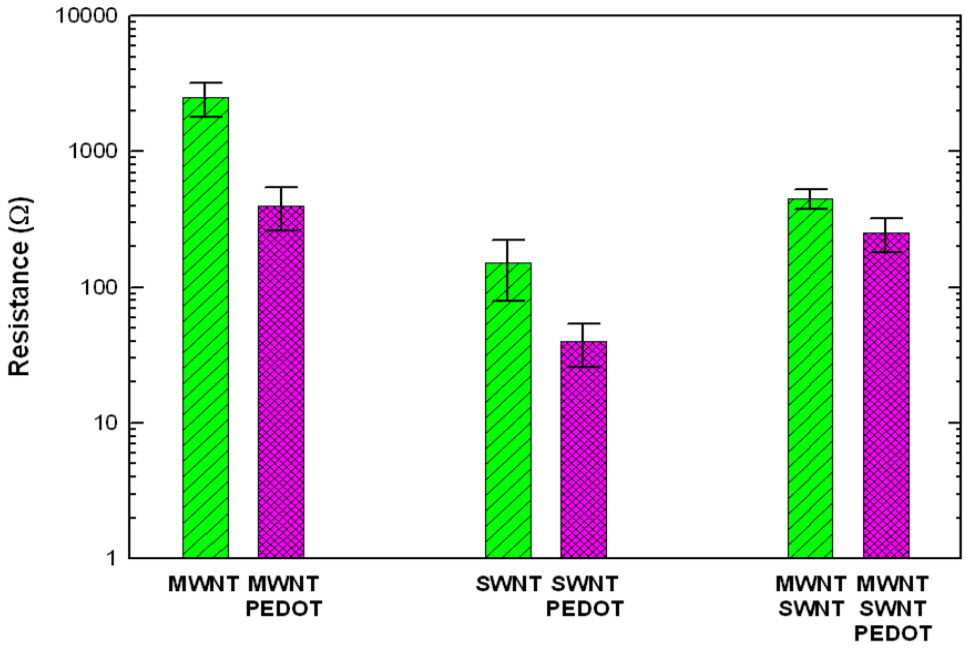

FIG. 11. Top-bottom electrical resistance change of cathode by adding conductive additives and conducting polymer

Figure 11 shows top-bottom resistance measurement results of cathodes which conductive additives and conducting polymer were added to. 90 : 5 : 5 ($LiCoO_2$: conductive additive : polymer binder) and 90 : 5 : 2.5 : 2.5 ($LiCoO_2$: conductive

additive : conducting polymer : polymer binder) weight ratio samples were used in this measurement. Top-bottom resistance of the no-conductive additives case (90 : 10, $LiCoO_2$: polymer binder, wt ratio) was 5 ~10 MΩ. Compared with the no-conductive additive case, the resistance of samples with added conductive additives was much lower. Among them, the cathode sample with added SWNTs as conductive additives had the lowest top-bottom resistance. In addition, top-bottom resistance could be reduced by adding conducting polymer. Thus, better electrically conductive networks can be made by adding conductive networks and conducting polymer.

3.1.2 Capacity measurement and result discussion

Current change and capacity change of Li-ion battery samples were measured during first charging. Voltage of samples before charging was about 0.4 ~ 0.6 V. Figures 12 and 13 show current and capacity change of the 90 : 5 : 5 ($LiCoO_2$: SWNTs : PVdF) wt ratio sample during first charging (1 hour). As can be seen figures 12 and 13, charging current and capacity was very small compared with other research results (about 140 mAh/g). In addition, the voltage of the sample was 2 ~ 3 V after charging, and it dropped quickly to the original voltage. Even though increasing the charging time to 3 hours, results were the same.

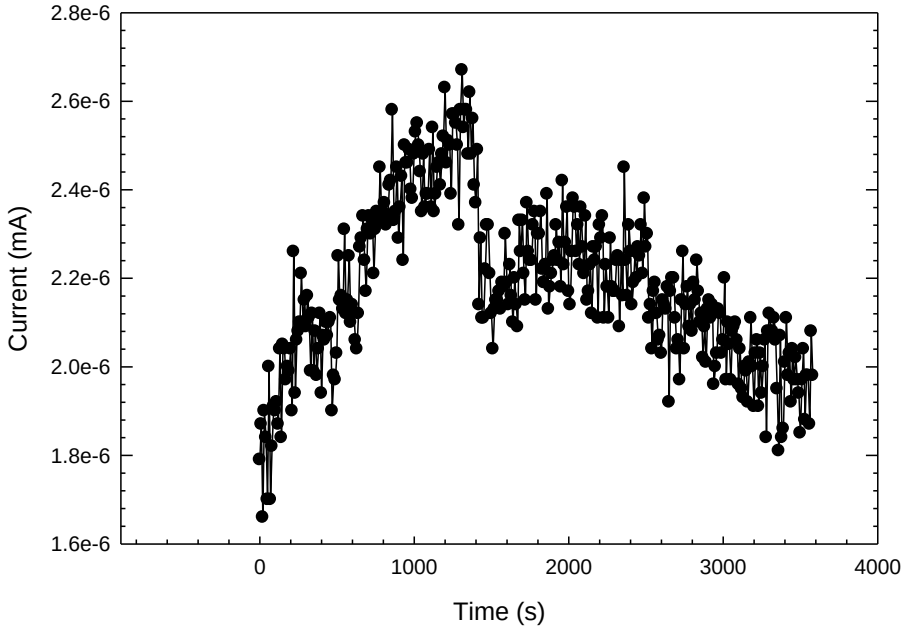

FIG. 12. Graph of current change during charging

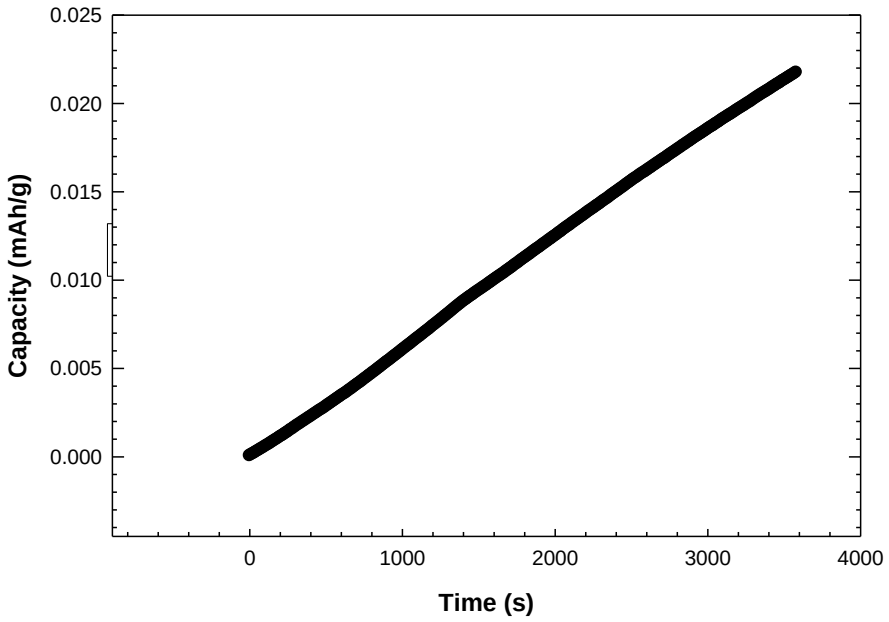

FIG. 13. Graph of capacity change during charging

Several factors might cause small capacity and voltage drop after charging. First, the performance of the Li-ion battery was limited because of lithium metal foil oxidation during assembly procedures. Although the glove box was vacuumed by pump, air including oxygen remained in the glove box because vacuum pump power was low. Lithium foil reacted with remaining oxygen so the surface changed into an oxide layer. As a result, transfer of lithium ion between cathode and anode was limited and capacity of battery was reduced.

Another reason can be found in the cathode. The cathode was made by pouring mixed cathode slurry onto aluminum foil and drying in the vacuum oven. During this procedure, mixed slurry was spread out on the foil, so the density of cathode was decreased. As a result, the amount of $LiCoO_2$ amount in the cathode was limited and capacity of battery was reduced.

Applied pressure to battery cases during assembly step can also be one reason for the limited capacity problem. An acrylic plate was used as battery case in this work due to simplicity of assembly. Acrylic plates were attached by epoxy without pressure in the assembly step. In other studies, commercial coin cells were used as battery case and a lot of pressure was applied to the coin cells during assembly. As a result, cathode and anode could be more closed due to applied pressure, so lithium ions can move easily between cathode and anode through electrolyte. Thus, the low capacity of cathode could be caused by low pressure during assembly step in this work.

In order to overcome these problems, several things should be applied to the work. First, a more powerful vacuum should be applied in the glove box to prevent

oxidation of lithium foil as anode. Graphite foil, of course, can be used as anode in stead of lithium foil due to its low reactivity with oxygen. Second, the density of the cathode must increase in order to improve capacity of battery. Using more viscous slurry during the cathode making step and applying pressure to the coated slurry on aluminum foil are possible methods to enhance the density of cathode. Finally, pressure should be applied to the battery case during assembly step to decrease the moving distance of lithium ion.

3.2 Thermal interface materials

3.2.1 Metal particles decorated MWNTs-polymer composites

In order to confirm the metal-particle-decorating effect for the thermal conductivity enhancement, iron- and nickel-particle-doped CNTs polymer composites were prepared. In figure 14, the TEM image shows how metal particles decorated on the surface of MWNTs. Many metal particles doped on the wall and junctions of MWNTs in the TEM image.

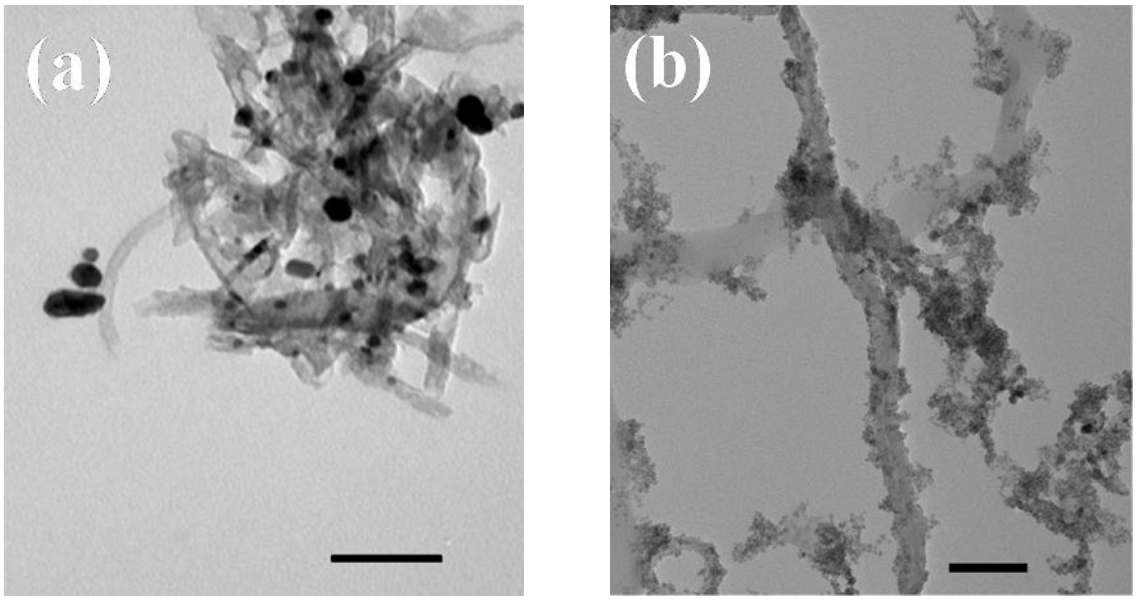

FIG. 14. TEM image of metal particles decorated on the surface of MWNTs (a) nickel particles decorated MWNTs, scale bar: 100 nm, (b) iron particles decorated MWNTs, scale bar: 100 nm

The thermal conductivity of iron- and nickel-particle-doped CNTs polymer composite was compared with MWNTs-polymer nanocomposites in figure 15. Thermal conductivity measurement results of metal-particle-decorated MWNTs were almost the same or slightly higher than only MWNTs-polymer nanocomposites. These results may be caused by difference of phonon conduction spectrum between metal particles and MWNTs or poor dispersion of metal-decorated MWNT during synthesis steps. Although surfactant was used for dispersion during sample synthesis step, metal-decorated MWNTs were not perfectly dispersed in water. In order to reduce the particle size and disperse in water, metal-particle-decorated MWNTs were ball milled. However, dispersion in water was slightly better than before ball milling. As a result, thermal conductivity of metal-particle-decorated MWNTs-polymer composites was not much improved.

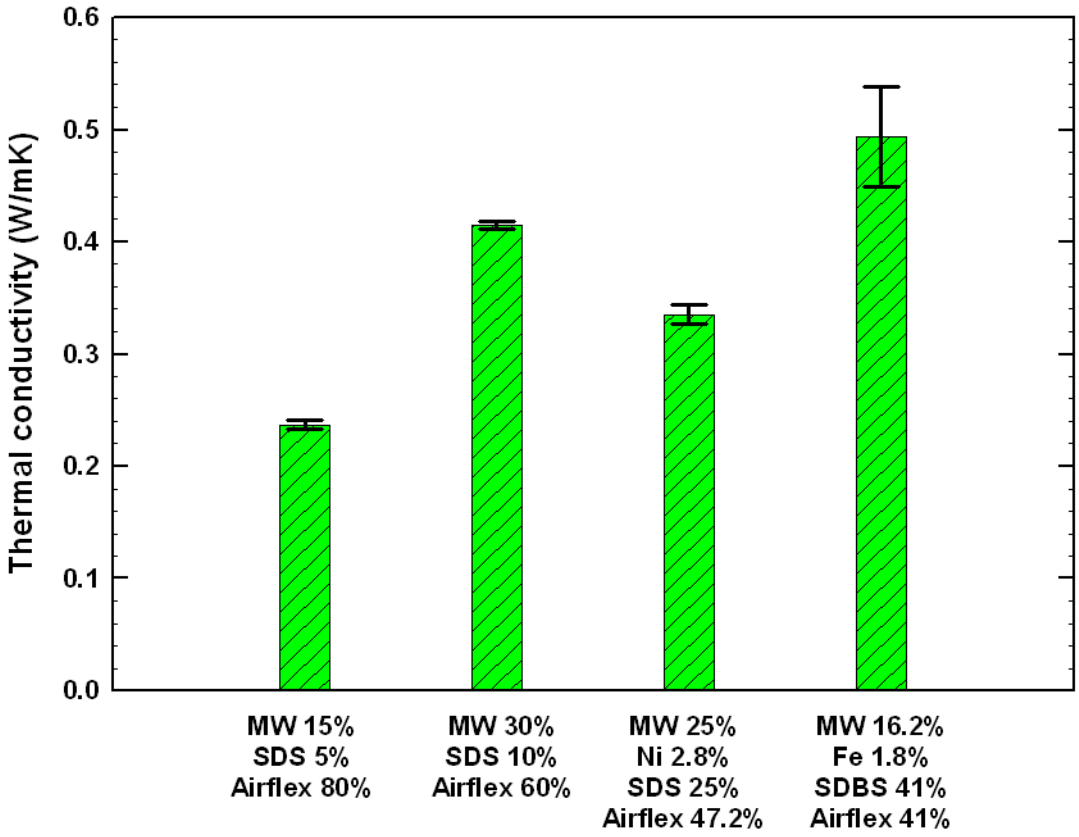

FIG. 15. Thermal conductivity comparison of MWNTs-polymer composites and metal particle decorated MWNTs-polymer composites (volume ratio)

3.2.2 Nanocomposites using different types of fillers

The thermal conductivity comparisons of MWNTs and graphite-polymer nanocomposites are shown in figure 16. MWNTs-polymer nanocomposites over 30% filler weight ratio could not be prepared due to split. Although MWNTs-polymer composite solution was dispersed well before drying, film was not formed because of MWNTs aggregation during drying.

In figure 16, the samples with a larger ratio of MWNTs or graphite to filler have higher thermal conductivity. Thermal conductivity of the MWNTs 30 % sample was increased by about 200 % compared to the MWNTs 15 % sample and also graphite 60 % sample was 2 times the value of the graphite 30 % sample. Overall, the thermal conductivity increased in along with the filler ratio in the composite.

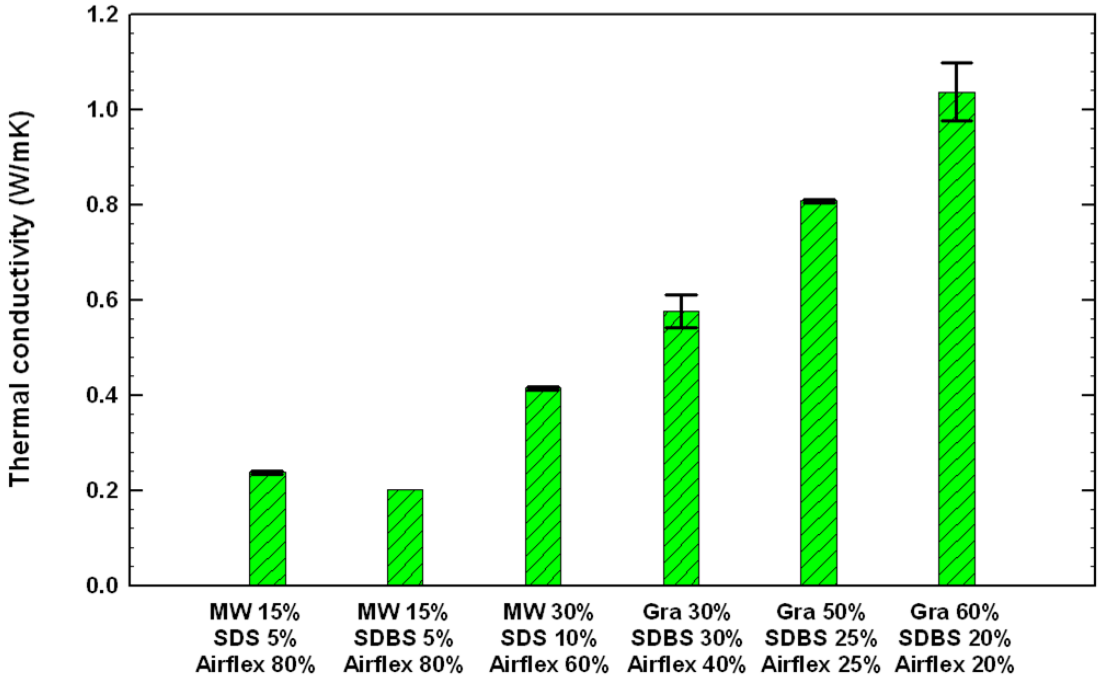

FIG. 16. Thermal conductivity comparison of MWNTs and graphite-polymer nanocomposites

The thermal conductivity of graphite-polymer nanocomposites was higher than MWNTs-polymer nanocomposites. The thermal conductivity of graphite 30 % sample was about 1.5 times higher than that of the MWNTs 30% sample. This result may be explained difference of filler structure. Because CNTs structure shape is circular and tube shaped, so CNTs structure have point junction in the polymer nanocomposite. Thus,

phonon conduction was limited due to small junctions. On the other hand, graphite has a flat surface. A graphite layer can be connected line or surface shape with different layers due to its flat surface. As a result, graphite have larger and more junctions than CNTs. Thus, because phonon transport is better in graphite, thermal conductivity of graphite-based composite can be improved.

In order to improve thermal conductivity of nanocomposites, MWNTs were added into graphite-polymer nanocomposites. 4 : 1 (Graphite : MWNTs, weight ratio), 1 : 1 and 1 : 4 samples were prepared to compare with the graphite 50 % sample. As can be seen in figure 17, thermal conductivity of nanocomposites was enhanced by adding MWNTs into graphite-polymer nanocomposites. The thermal conductivity of the 1 : 1 sample improved about 200 % compared with the graphite 50 % sample. In addition, the 1 : 1 sample had the best thermal conductivity value among MWNTs and graphite mixed samples.

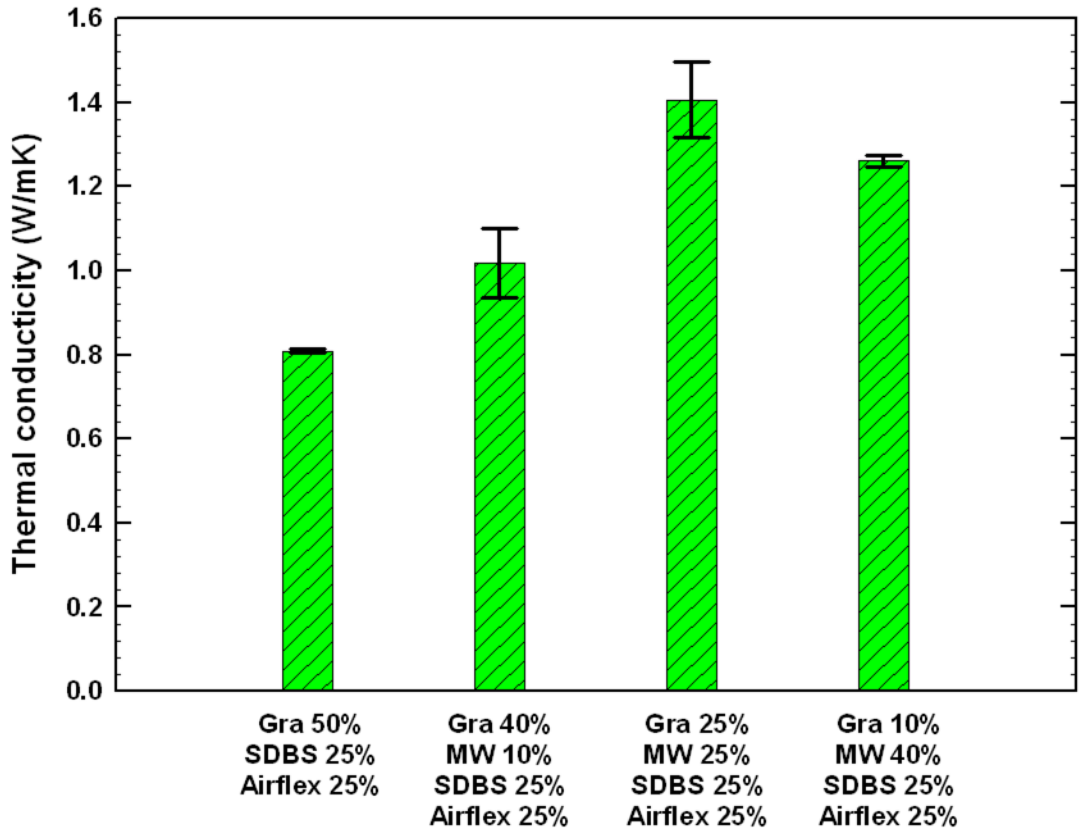

Fig. 17. Thermal conductivity change with MWNTs and graphite ratio in the nanocomposites

The thermal conductivity increase could be due to the presence more conductive network formation in the composite. As can be seen figure 18 (a), several graphite layers were stacked in the horizontal direction and there were some voids between graphite layers. However, the mixed filler sample in figure 18 (b) shows some MWNTs connection between graphite layers. Thus, by adding MWNTs into graphite-polymer nanocomposites, MWNTs may be located between graphite layers, so more phonon conduction can occur in the nanocomposite. As a result, thermal conductivity of MWNTs and graphite mixed nanocomposites can be improved.

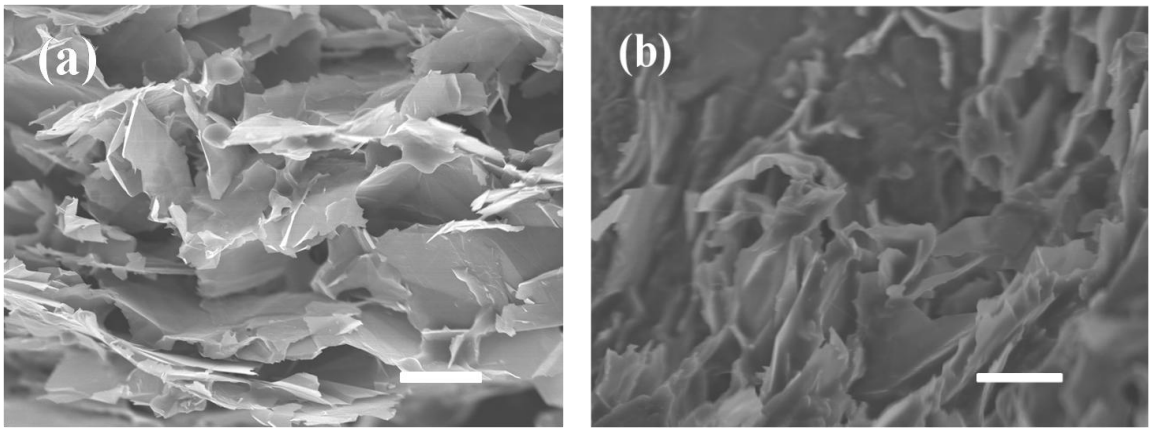

FIG. 18. SEM of (a) graphite-SDBS-Airflex (50 : 25 : 25, wt ratio) composite, scale bar: 5 μm and (b) graphite-MWNTs-SDBS-Airflex (25 : 25 : 25 : 25, wt ratio) composite cross section, scale bar: 5 μm

3.2.3 Nancomposites using different types of polymers

Thermal conductivity can be changed when a different polymer is applied to nanocomposites. EPON 862 was used as a polymer binder in nanocomposites in order to see thermal conductivity change compare with airflex. The thermal conductivity measurement results of 50 % graphite samples and MWNTs and graphite mixed samples (25 % : 25 %) which were EPON 862- and airflex-based nanocomposites were compared in figure 19. In figure 19, EPON 862-based nanocomposites showed higher thermal conductivity value than airflex-based nanocomposites. Thermal conductivity of EPON 862 based nanocomposites was enhanced about 0.6 ~ 0.8 W/mK compared with airflex based nanocomposites in both cases.

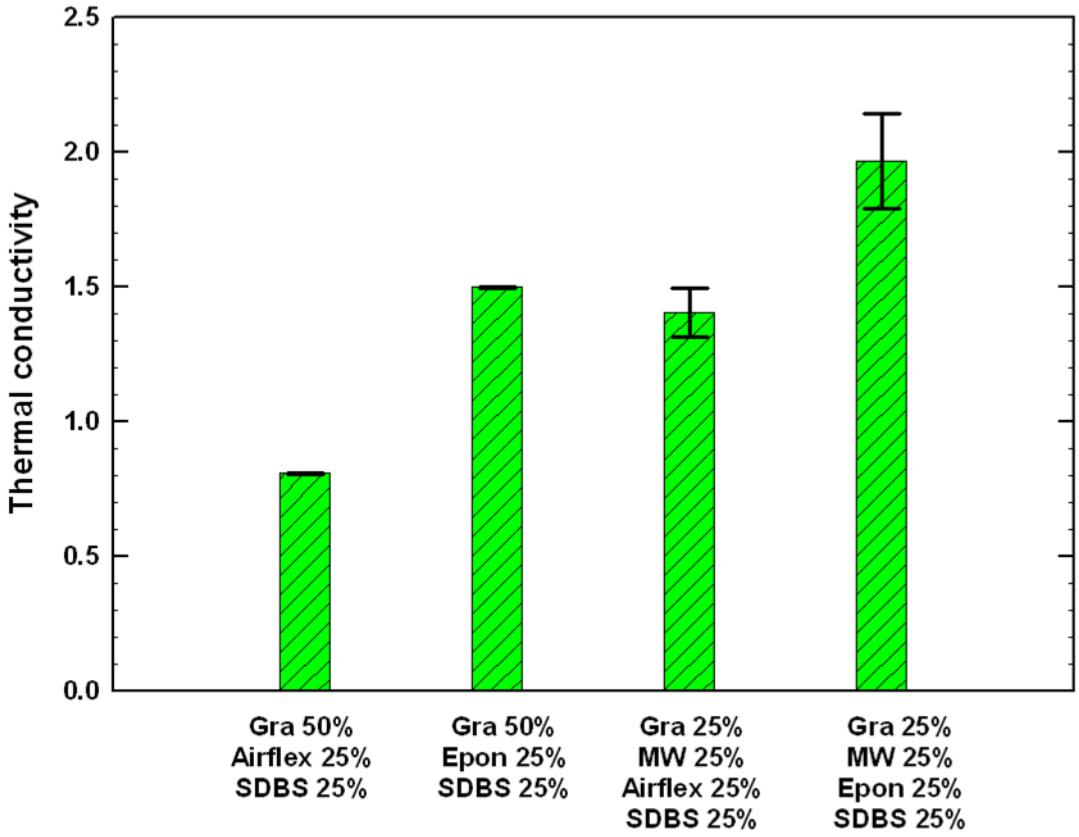

FIG. 19. Thermal conductivity comparison of polymer type (EPON vs Airflex)

Thrmal conductivity can be affected by the interfacial adhesion between filler and polymer. The strong adhesion between filler and polymer can hinder the phonon vibration at the interface. On the other hand, thermal conductance can be improved by the weak adhesion. Airflex based composites are more flexible than EPON 862 based sample due to low glass transition temperature (-15 ℃) and young's modulus of airflex. Airflex can attach onto filler to a greater extent than EPON 862 because of this property. As can be seen figure 20 (a), polymer is attached onto filler in airflex-based composites. However, a smaller amount of EPON is attached onto filler than airflex-based

composites in figure 20 (b). As a result, thermal conductivity of airflex-based composite is lower than EPON 862-based composite.

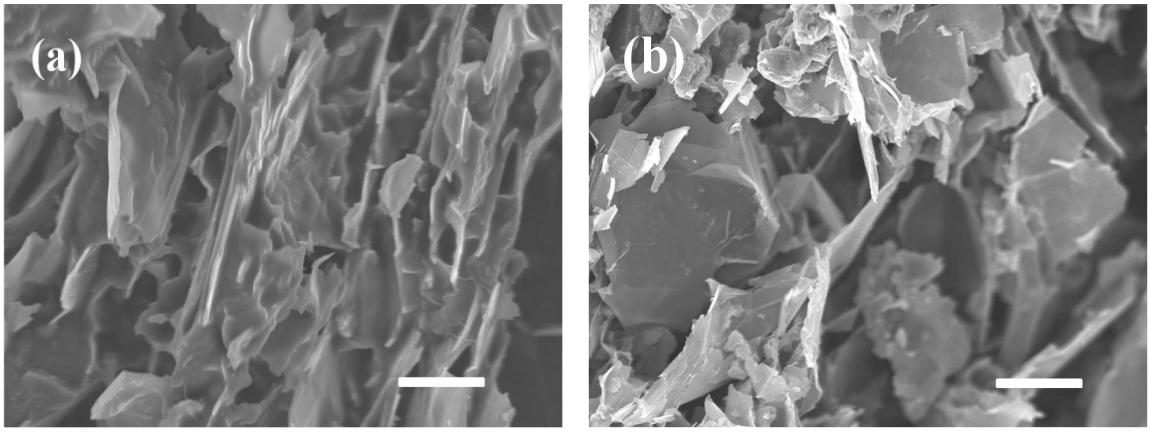

FIG. 20. SEM of (a) graphite-MWNTs-SDBS-Airflex (25 : 25 : 25 : 25, wt ratio) composite, scale bar: 5 μm and (b) graphite-MWNTs-SDBS-EPON (25 : 25 : 25 : 25, wt ratio) composite cross section, scale bar: 5 μm

3.2.4 Nanocomposites without surfactant

DMF or NMP was uesd to increase the filler ratio in the composites. MWNTs and graphite were dispersed well in a DMF or NMP solution without surfactant such as SDBS. In addition, a polymer such as airflex was dissolved in these solvents so MWNTs, graphite and polymer could be mixed in these solvents by sonication, finally being made into nanocomposites. Moreover, filler percentage of nanocomposites could be increased by this method because surfactant was not used in this method.

Figure 21 shows thermal conductivity results of samples using DMF. The samples with a larger ratio of filler have higher thermal conductivity. In addition, MWNTs mixed samples have slightly higher thermal conductivity than only graphite

samples. However, the thermal conductivity value was lower than with surfactant samples although filler percentage was increased.

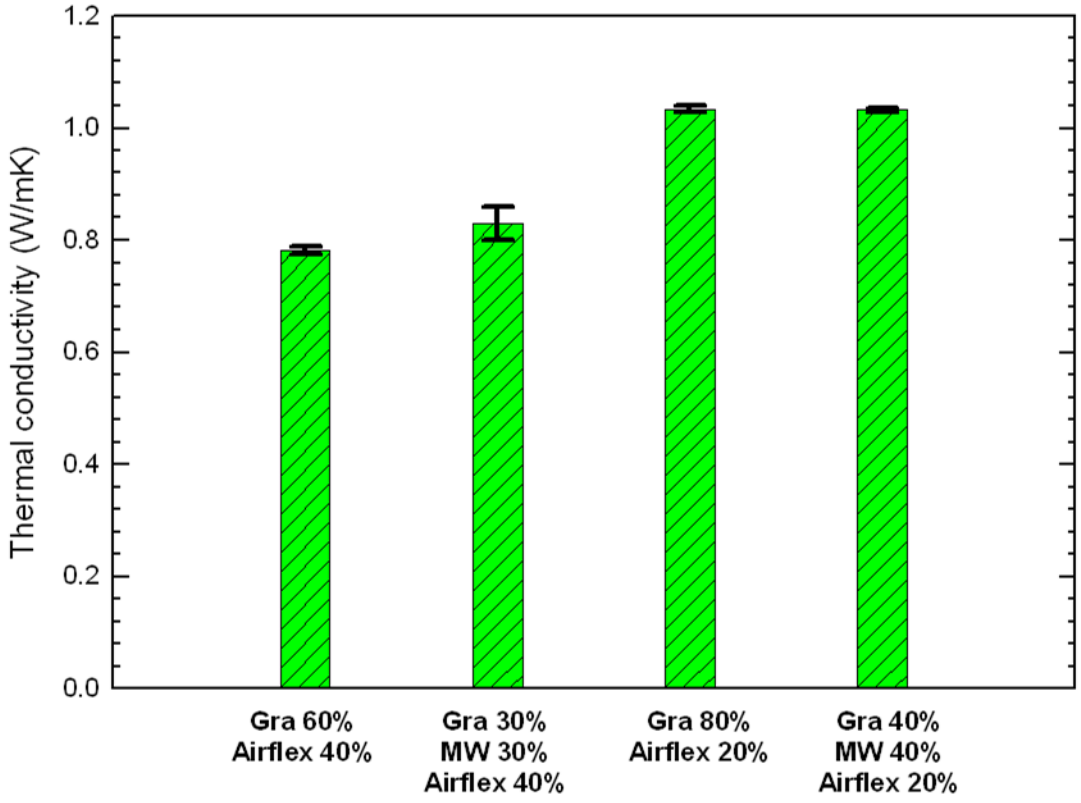

FIG. 21. Thermal conductivity measurement results of DMF using composites

NMP samples show higher thermal conductivity values than DMF samples, as seen in figure 22. In addition, thermal conductivity enhancement of mixed filler samples using NMP shows the same pattern with using surfactant samples. The 1 : 1 ratio sample shows the best thermal conductivity value compared with the graphite only and the 4 : 1 sample.

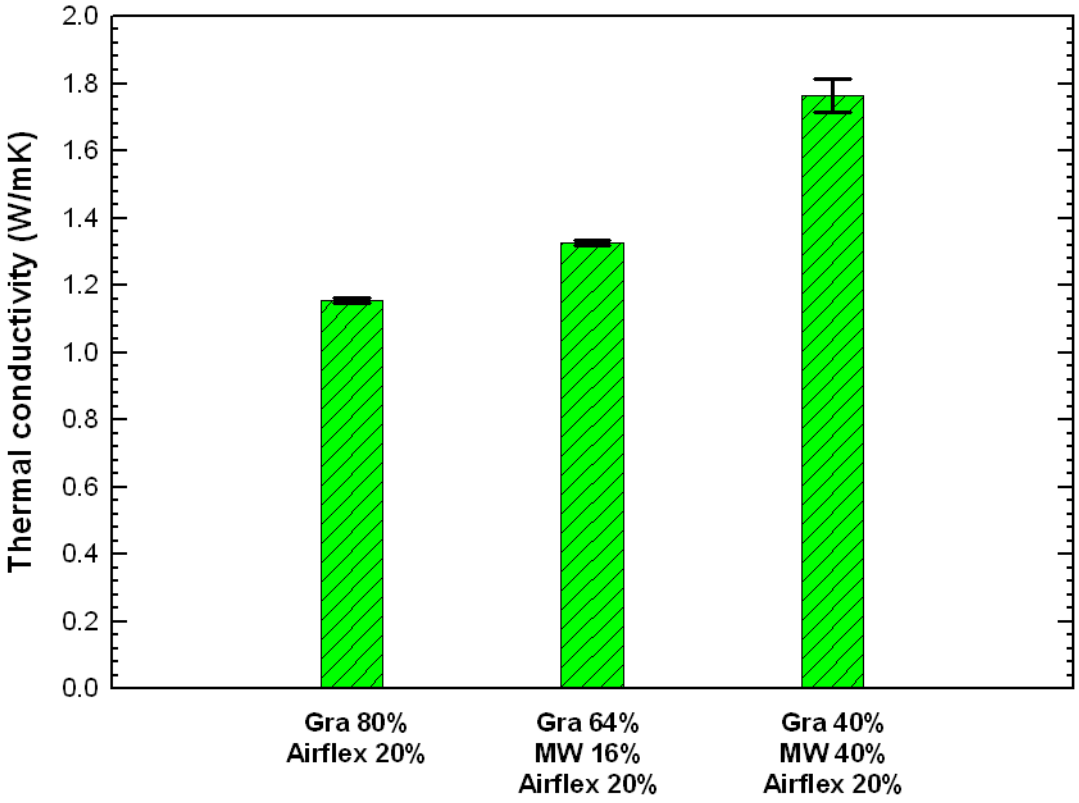

FIG. 22. Thermal conductivity measurement results of NMP using composites

The thermal conductivity difference between samples using DMF and NMP can be assumed from the SEM. In figure 23 (a), there are many voids between fillers indicating that the amount of polymer binder was insufficient in composites using DMF. On the other hand, voids in the structure of the NMP case were smaller than those in the DMF case and more polymer binder was in the compsoite in figure 23 (b). In the DMF case, Polymer binder might be melted by DMF, so voids occurred in the composite. As a result, the thermal conductivity of the DMF case was decreased compared with the NMP case due to voids in the structure.

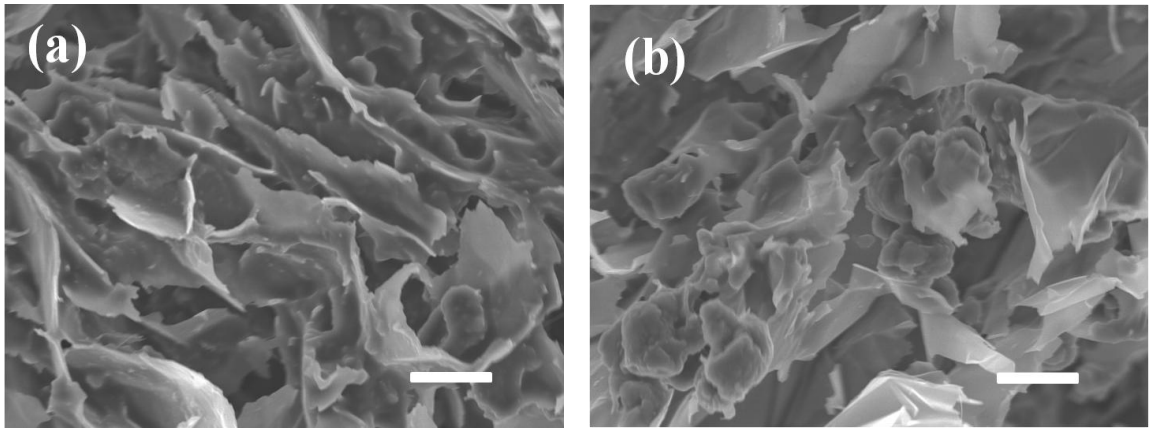

FIG. 23. SEM of (a) graphite-MWNTs-Airflex (40 : 40 : 20, wt ratio) composite using DMF, scale bar: 5 µm and (b) graphite-MWNTs-Airflex (40 : 40 : 20, wt ratio) composite using NMP cross section, scale bar: 5 µm

CHAPTER IV

CONCLUSION

Polymer-nanocomposites were synthesized by adding conductive additives and conducting polymer into the cathode in order to improve the electrochemical properties of Li-ion batteries. The electrical resistance was decreased by adding conductive additives and conducting polymer into the cathode. However, the capacity and voltage of the Li-ion cell could not be enhanced because of oxidation of the anode, low density of cathode and long moving distance of the lithium ions. In order to overcome these problems, graphite foil can be used as anode instead of lithium foil. By using more viscous slurry and applying press coating during cathode production step, low cathode density problem can be fixed. In addition, problem of the long moving distance of lithium ions can be overcome by applying pressure during the cell assembly step.

The thermal conductivity of polymer-nanocomposites can be enhanced using several methods. Graphite, MWNTs and mixed filler-polymer composites were prepared and then thermal conductivity measured to confirm the filler effects. In the mixed filler-polymer case, 4 : 1 (MWNTs : graphite), 1 : 1 and 1 : 4 weight-ratio samples were prepared to find the optimal ratio. In addition, several polymer nanocomposites were synthesized to observe metal particle decorating effect, different polymer effect and surfactant effect.

As a result of measurements, it is clear that thermal conductivity of polymer nanocomposites can be enhanced by using graphite as filler. In addition, by adding

MWNTs into graphite-polymer nanocomposites, thermal conductivity can be greatly improved. Futhermore, thermal conductivity of nanocomposites can be enhanced using different polymers and decorating with metal particles. Finally, polymer-nanocomposites can be synthesized using solvents without surfactant and thermal conductivity can be changed by using different solvents.

REFERENCES

[1] M. F. Yu, B. S. Files, S. Arepalli, and R. S. Ruoff, Physical Review Letters **84,** 5552 (2000).

[2] J. Hone, M. C. Llaguno, M. J. Biercuk, A. T. Johnson, B. Batlogg, Z. Benes, and J. E. Fischer, Applied Physics a-Materials Science & Processing **74,** 339 (2002).

[3] S. Berber, Y. K. Kwon, and D. Tomanek, Physical Review Letters **84,** 4613 (2000).

[4] D. J. Yang, S. G. Wang, Q. Zhang, P. J. Sellin, and G. Chen, Physics Letters A **329,** 207 (2004).

[5] A. Thess, R. Lee, P. Nikolaev, H. J. Dai, P. Petit, J. Robert, C. H. Xu, Y. H. Lee, S. G. Kim, A. G. Rinzler, D. T. Colbert, G. E. Scuseria, D. Tomanek, J. E. Fischer, and R. E. Smalley, Science **273,** 483 (1996).

[6] P. Nikolaev, M. J. Bronikowski, R. K. Bradley, F. Rohmund, D. T. Colbert, K. A.Smith, and R. E. Smalley, Chemical Physics Letters **313,** 91 (1999).

[7] J. H. Du, J. Bai, and H. M. Cheng, Express Polymer Letters **1,** 253 (2007).

[8] G. Nazri and G. Pistoia, *Lithium batteries : science and technology* (Kluwer Academic Publishers, Boston, 2004).

[9] E. Antolini, Solid State Ionics **170,** 159 (2004).

[10] D. Belov and M. H. Yang, Solid State Ionics **179,** 1816 (2008).

[11] D. Belov and M. H. Yang, Journal of Solid State Electrochemistry **12,** 885 (2008).

[12] C. H. Doh, D. H. Kim, H. S. Kim, H. M. Shin, Y. D. Jeong, S. I. Moon, B. S. Jin, S. W. Eom, H. S. Kim, K. W. Kim, D. H. Oh, and A. Veluchamy, Journal of Power Sources **175,** 881 (2008).

[13] G. G. Amatucci, J. M. Tarascon, and L. C. Klein, Solid State Ionics **83,** 167 (1996).

[14] G. G. Amatucci, J. M. Tarascon, and L. C. Klein, Journal of the Electrochemical Society **143,** 1114 (1996).

[15] T. Amriou, B. Khelifa, H. Aourag, S. M. Aouadi, and C. Mathieu, Materials Chemistry and Physics **92,** 499 (2005).

[16] H. S. Liu, Y. Yang, and J. J. Zhang, Journal of Power Sources **173,** 556 (2007).

[17] A. Rougier, P. Gravereau, and C. Delmas, Journal of the Electrochemical Society **143,** 1168 (1996).

[18] D. C. Li, Z. H. Peng, H. B. Ren, W. Y. Guo, and Y. H. Zhou, Materials Chemistry and Physics **107,** 171 (2008).

[19] M. S. Whittingham, Chemical Reviews **104,** 4271 (2004).

[20] A. K. Padhi, K. S. Nanjundaswamy, and J. B. Goodenough, Journal of the Electrochemical Society **144,** 1188 (1997).

[21] J. W. Fergus, Journal of Power Sources **195,** 939 (2010).

[22] C. K. Chan, X. F. Zhang, and Y. Cui, Nano Letters **8,** 307 (2008).

[23] R. Ruffo, S. S. Hong, C. K. Chan, R. A. Huggins, and Y. Cui, Journal of Physical Chemistry C **113,** 11390 (2009).

[24] D. Im and A. Manthiram, Solid State Ionics **159,** 249 (2003).

[25] J. M. Tarascon and M. Armand, Nature **414,** 359 (2001).

[26] Y. Idota, T. Kubota, A. Matsufuji, Y. Maekawa, and T. Miyasaka, Science **276,** 1395 (1997).

[27] Y. Wang and G. Z. Cao, Advanced Materials **20,** 2251 (2008).

[28] Y. H. Chen, C. W. Wang, G. Liu, X. Y. Song, V. S. Battaglia, and A. M. Sastry, Journal of the Electrochemical Society **154,** A978 (2007).

[29] J. K. Hong, J. H. Lee, and S. M. Oh, Journal of Power Sources **111,** 90 (2002).

[30] D. H. Jang and S. M. Oh, Electrochimica Acta **43,** 1023 (1998).

[31] J. Shirakawa, M. Nakayama, H. Ikuta, Y. Uchimoto, and M. Wakihara, Electrochemical and Solid State Letters **7,** A27 (2004).

[32] C. Sotowa, G. Origi, M. Takeuchi, Y. Nishimura, K. Takeuchi, I. Y. Jang, Y. J. Kim, T. Hayashi, Y. A. Kim, M. Endo, and M. S. Dresselhaus, Chemsuschem **1,** 911 (2008).

[33] K. Sheem, Y. H. Lee, and H. S. Lim, Journal of Power Sources **158,** 1425 (2006).

[34] M. Endo, Y. A. Kim, T. Hayashi, K. Nishimura, T. Matusita, K. Miyashita, and M. S. Dresselhaus, Carbon **39,** 1287 (2001).

[35] G. P. Wang, Q. T. Zhang, Z. L. Yu, and M. Z. Qu, Solid State Ionics **179,** 263 (2008).

[36] C. Yu, Y. S. Kim, D. Kim, and J. C. Grunlan, Nano Letters **8,** 4428 (2008).

[37] F. Sarvar, D. C. Whalley, and P. P. Conway, ESTC 2006: 1st Electronics Systemintegration Technology Conference, Vols 1 and 2, Proceedings**,** 1292 (2006).

[38] S. Narumanchi, M. Mihalic, K. Kelly, and G. Eesley, 2008 11th IEEE Intersociety Conference on Thermal and Thermomechanical Phenomena in Electronic Systems, Vols 1-3**,** 395 (2008).

[39] R. Prasher, Proceedings of the Ieee **94,** 1571 (2006).

[40] X. J. Hu, L. N. Jiang, and K. E. Goodson, Itherm 2004, Vol 1**,** Proceedings, 63 (2004).

[41] B. Vigolo, A. Penicaud, C. Coulon, C. Sauder, R. Pailler, C. Journet, P. Bernier, and P. Poulin, Science **290,** 1331 (2000).

[42] F. H. Gojny, M. H. G. Wichmann, B. Fiedler, I. A. Kinloch, W. Bauhofer, A. H. Windle, and K. Schulte, Polymer **47,** 2036 (2006).

[43] T. Kashiwagi, E. Grulke, J. Hilding, K. Groth, R. Harris, K. Butler, J. Shields, S. Kharchenko, and J. Douglas, Polymer **45,** 4227 (2004).

[44] W. Kim, R. Wang, and A. Majumdar, Nano Today **2,** 40 (2007).

[45] E. E. Marotta, S. J. Mazzuca, and J. Norley, IEEE Transactions on Components and Packaging Technologies **28,** 102 (2005).

[46] M. Smalc, J. Norley, R. A. Reynolds, R. Pachuta, and D. W. Krassowski, Advances in Electronic Packaging 2003, Vol 2**,** 253 (2003).

[47] B. Debelak and K. Lafdi, Carbon **45,** 1727 (2007).

[48] A. P. Yu, P. Ramesh, M. E. Itkis, E. Bekyarova, and R. C. Haddon, Journal of Physical Chemistry C **111,** 7565 (2007).

[49] S. D. Bergin, V. Nicolosi, P. V. Streich, S. Giordani, Z. Y. Sun, A. H. Windle, P. Ryan, N. P. P. Niraj, Z. T. T. Wang, L. Carpenter, W. J. Blau, J. J. Boland, J. P. Hamilton, and J. N. Coleman, Advanced Materials **20,** 1876 (2008).

[50] J. Wang, D. Fruchtl, and W. J. Blau, Optics Communications **283,** 464 (2010).

VITA

Name:	Wonchang Park
Address:	Department of Mechanical Engineering, 3123, TAMU, College Station, Texas, 77843-3123, USA.
Email Address:	pwcking@gmail.com
Education:	B.S., Environmental Science, Korea Military Academy, 2005 M.S., Mechanical Engineering, Texas A&M University, 2009